# The instability and acoustic wave modes of supersonic mixing layers inside a rectangular channel

## By CHRISTOPHER K. W. TAM AND FANG Q. HU

Department of Mathematics, Florida State University, Tallahassee, FL 32306-3027, USA

(Received 29 February 1988 and in revised form 6 October 1988)

At high supersonic convective Mach numbers the familiar Kelvin-Helmholtz instability of a thin unconfined two-dimensional shear layer becomes neutrally stable. In this paper, it is shown that when the same shear layer is put inside a rectangular channel the coupling between the motion of the shear layer and the acoustic modes of the channel produces new two-dimensional instability waves. The instability mechanism of these waves is examined. Extensive numerical computation of the properties of these new instability waves has been carried out. Based on these results two classes of these waves are identified. Some of the important characteristic features of these waves are reported in this paper. In addition to the unstable waves, a thorough analysis of the normal modes of a supersonic shear layer inside a rectangular channel reveals that there are basically two other families of neutral acoustic waves. Examples of some of the prominent characteristics of these neutral acoustic waves are also provided in this paper. The new instability waves are the dominant instabilities of a confined mixing layer at high supersonic convective Mach number. As such they are very relevant to the supersonic mixing and combustion processes inside a ramjet engine combustion chamber.

#### 1. Introduction

Recently there has been a growing interest in acquiring a better understanding of the underlying processes involved in supersonic mixing and combustion. Experimentally it has been found, for example by Ikawa & Kubota (1975), Bogdanoff (1983), Papamoschou & Roshko (1986) and Chinzei et al. (1986), that the spreading or mixing rates of supersonic shear layers are considerably less than those at subsonic speeds. The decrease is attributed to the effect of compressibility. Bogdanoff and Papamoschou & Roshko suggested that the proper parameter to use as a measure of compressibility effect is the 'convective Mach number', which is defined as the Mach number of the flow measured in a moving frame of reference fixed to the dominant waves or large structures of the mixing layers. As the convective Mach number increases, the spreading rate of a mixing layer decreases. At supersonic convective Mach numbers the spreading rate is a factor of four or five smaller than that at incompressible conditions. In an effort to provide a plausible reason for the decrease in spreading rate with increase in convective Mach number Papamoschou & Roshko (1986) demonstrated that both the normalized Kelvin-Helmholtz instability growth rate and the normalized spreading rate of two-dimensional mixing layers have identical dependence on convective Mach number. The implication is that the decrease in mixing rate is directly related to the decrease in the growth of the instability of the mixing layer as the convective Mach number increases.

Earlier Miles (1958) used a vortex-sheet model to study the two-dimensional instabilities of free shear layers. He showed that at high supersonic convective Mach number a shear layer became neutrally stable. Subsequent work by Lessen, Fox & Zien (1965), Gropengiesser (1970), Blumen, Drazin & Billings (1975), Tam & Morris (1980) and others using finite-mixing-layer models conclusively demonstrated that the Kelvin-Helmholtz instability, which was the principal instability of the shear layers, became less and less unstable as convective Mach number increased. In all the above investigations the shear layers were assumed to be free and unconfined. In the case of supersonic mixing layers inside a rectangular channel such as those in a ramjet combustor, the situation is quite different. The unsteady motion of the shear layer is invariably coupled to the acoustic modes of the rectangular channel through reflections of the acoustic waves by the channel walls. One of the primary objectives of this paper is to show that at supersonic convective Mach number the coupled motion produces new families of hydrodynamic instabilities. These instabilities will be referred to as supersonic instabilities in the rest of this paper. Further, at these flow conditions the new instabilities are the dominant instabilities of the flow.

In contrast to instabilities of shear layers in an open environment, there is an absence of analytical studies of the instabilities and wave modes of confined high-speed shear layers. Inside a rectangular channel the motion of a shear layer produces both unstable and neutral wave modes. A second objective of this work is to study the characteristics of and to classify all these wave modes. In the course of carrying out the classification of these waves into appropriate families an interesting pole merging phenomenon in the complex wavenumber space was observed. Detailed mapping, however, shows that these are not absolute instabilities in the sense of Landau & Lifshitz (1959) and Briggs (1964). A discussion of this pole merging phenomenon and its interpretation will be given in a later section of this paper.

Before proceeding to the analysis of the instabilities of a two-dimensional shear layer inside a rectangular channel it is instructive first to examine the physical mechanism that causes a shear layer to become unstable. Here for simplicity it will be assumed that the mixing layer can be modelled adequately by a vortex sheet. In order to show the difference between the supersonic instability waves of confined shear layers mentioned above and the Kelvin–Helmholtz instability, the Ackeret's explanation (see Liepmann & Puckett 1947; Papamoschou & Roshko 1986) of the Kelvin–Helmholtz instability mechanism will first be briefly reviewed.

Consider a mixing layer separating flows at subsonic convective Mach numbers. In the stationary frame of reference let  $u_1$  and  $u_2(u_1>u_2)$  be the flow velocities on the two sides of the vortex sheet and  $c(u_2< c< u_1)$  be the phase velocity of the instability wave. Ackeret suggested that one should look at the flow in the wave frame of reference, i.e. a moving frame travelling at the same velocity as the wave (see figure 1a). Now in the wave frame of reference the flow in the upper half-plane is simply a uniform flow over a wavy wall. At subsonic convective Mach number the pressure is lowest at the crests of the wavy wall and highest at the troughs (see Liepmann & Roshko 1957, Chapter 8). Similar considerations may also be applied to the flow in the lower half-plane. Again the pressure is lowest at the crests and highest at the troughs of the wavy wall. Since the crests and troughs interchange on the two sides of the vortex sheet the net result is that a pressure imbalance exists across the vortex sheet. This pressure imbalance is in phase with the vortex-sheet displacement and hence would tend to increase its amplitude, leading to the well-known Kelvin–Helmholtz instability.

Suppose the convective Mach numbers are supersonic as shown in figure 1(b). The

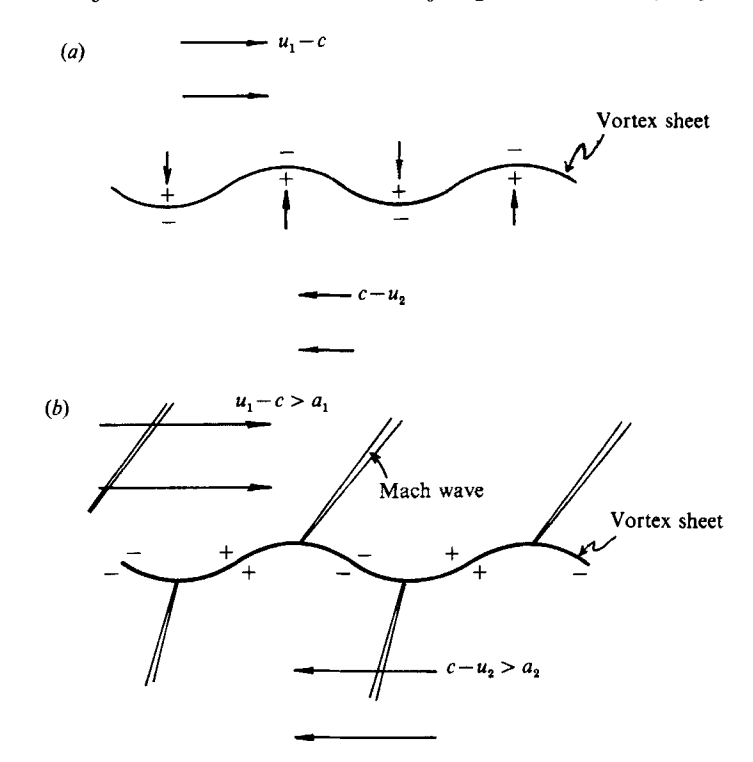


FIGURE 1. Kelvin-Helmholtz instability mechanism as viewed in the wave frame of reference: +, high-pressure region; -, low pressure region. (a) Subsonic convective Mach numbers, (b) supersonic convective Mach numbers.

pressure distribution associated with uniform supersonic flow over a wavy wall is 90° out of phase with the displacement of the wall. This results in identical pressure distributions on both sides of the vortex sheet. The net effect is that the wave becomes neutrally stable. This is in agreement with the prediction of hydrodynamic stability theory (see Miles 1958). Now if the mixing layer is confined inside a rectangular channel the situation is drastically altered by the presence of the walls. At supersonic convective Mach numbers, standing Mach wave systems can be sustained between the mixing layer and the walls by reflection as shown in figure 2. The pressure distribution on a wavy wall due to a Mach wave system is given in the Appendix. It is easy to show that the pressure difference exerted on the vortex sheet by the two Mach wave systems above and below is again in phase with the displacement of the wavy wall. As in the case of subsonic flow, the pressure imbalance at an appropriate wavelength will again tend to increase the amplitude of the sinusoidal displacement of the vortex sheet and thus lead to flow instability.

One of the special features of the supersonic instability waves is that there are many such wave modes. This is to be expected since many standing Mach wave patterns can be fitted in between the shear layer and the channel walls. Each of these patterns can give rise to an instability wave mode.

In §2 of this paper the instability problem of a two-dimensional shear layer inside a rectangular channel is formulated. The shear layer is modelled first by a vortex sheet. The effect of finite shear-layer thickness is then considered by incorporating realistic mean velocity, density and species concentration profiles in the governing

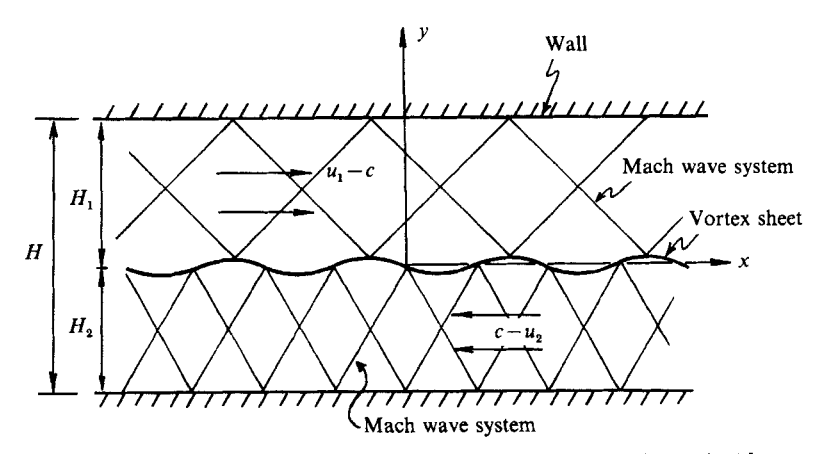


FIGURE 2. Mach wave systems associated with a thin wavy mixing layer inside a rectangular channel at supersonic convective Mach number flow conditions, as viewed in the wave frame of reference.

equations. In §3, the computation procedure needed to handle a large number of wave modes in the complex wavenumber space is discussed. It is shown that at supersonic convective Mach numbers all the instabilities are convective. Although a pole merging phenomenon occurs, the poles do not give rise to absolute instability. Typical numerical results of supersonic instability waves are given in §4. A case for which the vortex-sheet shear layer is neutrally stable, if unconfined because the convective Mach numbers are highly supersonic, is considered. It is found that, when housed inside a rectangular channel, the same shear layer becomes unstable and supports two classes of supersonic instabilities. The characteristics of these instability waves such as phase velocities, growth rates and finite shear-layer thickness effects are provided and discussed. In addition, it is found that the coupled motion between a shear layer and the acoustic modes of the rectangular channel also gives rise to two families of neutral waves. Some features of these waves are highlighted in this section.

## 2. Formulation and solution

In this paper the motion of a shear layer inside a rectangular channel separating two supersonic streams of gases will be studied by using a vortex-sheet model as well as a finite thickness mixing-layer model. The advantage of the vortex-sheet model is that a closed-form solution of the dispersion relation can be found. It turns out that the dispersion function is relatively simple. This allows extensive numerical computations by means of a grid-search technique to locate all the poles (zeros of the dispersion function) in the complex wavenumber space. For shear layers with finite thickness the dispersion relation can only be calculated numerically. Here this is done iteratively by Newton's method using the vortex-sheet solution as a starting value.

## 2.1. Vortex-sheet model

Consider small-amplitude motion associated with two supersonic fluid streams separated by a vortex sheet inside a rectangular channel of depth H and breadth B as shown in figure 3(a). For clarity, subscripts 1 and 2 will be used to designate

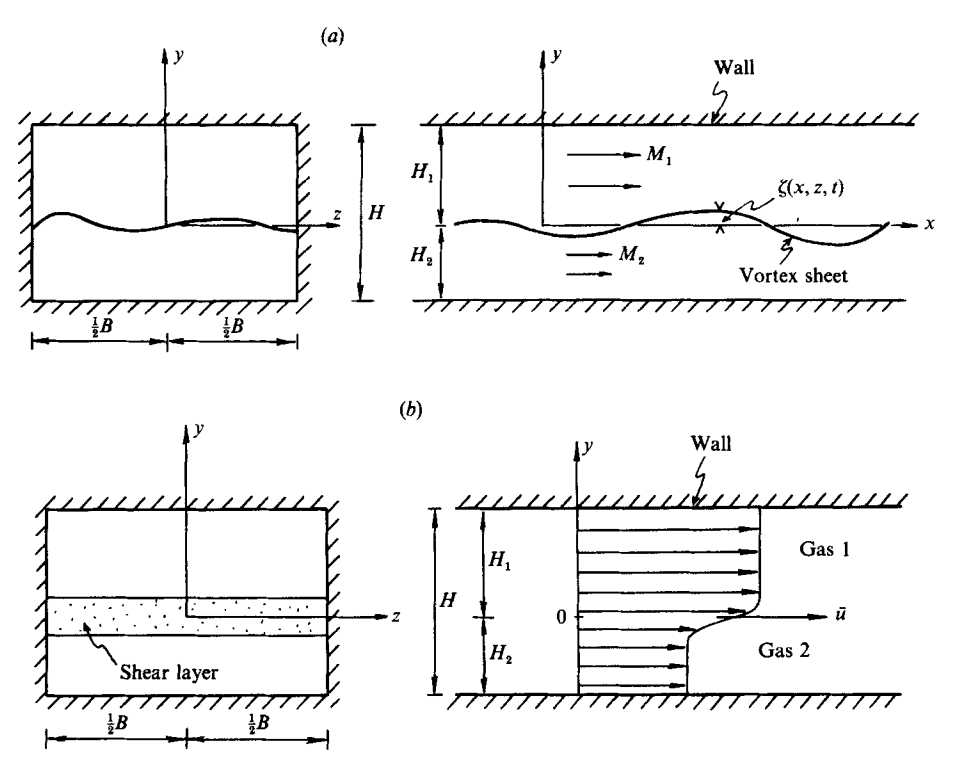


FIGURE 3. Flow models. (a) Vortex-sheet model of a confined shear layer. (b) Velocity profile of finite-thickness shear-layer model.

variables associated with the fluid stream above and below the vortex sheet respectively. The mean flow is assumed to be in static equilibrium with pressure balance, i.e.  $\bar{p}_1 = \bar{p}_2$  (p = pressure; overbar denotes mean flow quantity). On starting from the linearized continuity, momentum and energy equations of a compressible, inviscid fluid it is straightforward to find after eliminating all other variables that the perturbation pressures in regions 1 and 2 are governed by the convective wave equation:

$$\left( \frac{\partial}{\partial t} + \overline{u}_1 \frac{\partial}{\partial x} \right)^2 p_1 - \overline{a}_1^2 \nabla^2 p_1 = 0 \quad (0 < y \leqslant H_1),$$
 (2.1)

$$\left( \frac{\partial}{\partial t} + \overline{u}_2 \frac{\partial}{\partial x} \right)^2 p_2 - \overline{a}_2^2 \nabla^2 p_2 = 0 \quad (-H_2 \leqslant y < 0), \tag{2.2}$$

where  $\bar{u}$  and  $\bar{a}$  are the mean flow velocity and the speed of sound respectively.

Let  $y = \zeta(x, z, t)$  be the displaced position of the vortex sheet. Then the linearized dynamic and kinematic boundary conditions at the vortex sheet are

$$p_1(x, 0, z, t) = p_2(x, 0, z, t) \quad (y = 0),$$
 (2.3)

$$\left(\frac{\partial}{\partial t} + \overline{u}_1 \frac{\partial}{\partial x}\right)^2 \zeta = -\frac{1}{\overline{\rho}_1} \frac{\partial p_1}{\partial y}, \tag{2.4}$$

$$\left(\frac{\partial}{\partial t} + \bar{u}_2 \frac{\partial}{\partial x}\right)^2 \zeta = -\frac{1}{\bar{\rho}_2} \frac{\partial p_2}{\partial y}.$$
 (2.5)

The boundary conditions at the walls require

$$\frac{\partial p_1}{\partial y}(x,H_1,z,t)=0, \quad \frac{\partial p_2}{\partial y}(x,-H_2,z,t)=0, \tag{2.6} \label{eq:2.6}$$

$$\frac{\partial p_1}{\partial z}(x,y,\pm \frac{1}{2}B,t) = 0, \quad \frac{\partial p_2}{\partial z}(x,y,\pm \frac{1}{2}B,t) = 0. \tag{2.7}$$

To examine the stability characteristics of the flow, a wave solution of the following form which satisfies boundary condition (2.7) will now be sought:

$$\begin{pmatrix} p_1 \\ p_2 \\ \zeta \end{pmatrix} = \begin{pmatrix} \hat{p}_1(y) \\ \hat{p}_2(y) \\ \hat{\zeta} \end{pmatrix} e^{i(kx - \omega t)} \cos\left(\frac{2m\pi z}{B}\right) \quad (m = 0, 1, 2, 3, \ldots). \tag{2.8}$$

Substitution of (2.8) into (2.1) and (2.2) yields ordinary differential equations for  $\hat{p}_1$  and  $\hat{p}_2$ . The solutions of these equations that satisfy boundary condition (2.6) are

$$\hat{p}_1 = A\cos[\lambda_1(H_1 - y)], \quad \hat{p}_2 = C\cos[\lambda_2(y + H_2)], \tag{2.9}$$

where

$$\lambda_{1} = \left[ (\omega - \overline{u}_{1} k)^{2} / \overline{a}_{1}^{2} - k^{2} - (2\pi m/B)^{2} \right]^{\frac{1}{2}}$$

$$\lambda_{2} = \left[ (\omega - \overline{u}_{2} k)^{2} / \overline{a}_{2}^{2} - k^{2} - (2\pi m/B)^{2} \right]^{\frac{1}{2}}$$

$$(m = 0, 1, 2, 3, ...).$$

$$(2.10)$$

The branch cuts for  $\lambda_1$  and  $\lambda_2$  are chosen so that

$$0 \le \arg(\lambda_1), \arg(\lambda_2) < \pi. \tag{2.11}$$

Finally, upon substituting (2.8) and (2.9) into the dynamic and kinematic boundary conditions (2.3)–(2.5), the condition for the existence of a non-trivial solution leads to the following dispersion relation:

$$D \equiv \frac{\overline{a}_2^2 \lambda_2}{\gamma_2 (\omega - \overline{u}_2 \, k)^2} \sin{(\lambda_2 H_2)} \cos{(\lambda_1 H_1)} + \frac{\overline{a}_1^2 \lambda_1}{\gamma_1 (\omega - \overline{u}_1 \, k)^2} \sin{(\lambda_1 H_1)} \cos{(\lambda_2 H_2)} = 0, \eqno(2.12)$$

where  $\gamma$  is the ratio of specific heats.

# 2.2. Transformation to an equivalent two-dimensional case

Dispersion relation (2.12) includes all the three-dimensional wave modes. It is easy to show that the three-dimensional dispersion function characterized by the lateral mode number m can be transformed to an equivalent two-dimensional case by the following change of variables. Let

$$k^* = \left[1 + \frac{(2m\pi)^2}{(Bk)^2}\right]^{\frac{1}{2}}k, \quad \bar{u}_1^* = \frac{\bar{u}_1 k}{k^*}, \quad \bar{u}_2^* = \frac{\bar{u}_2 k}{k^*}$$
 (2.13)

The two-dimensional equivalent of the dispersion function is

$$D^* = \frac{\bar{a}_1^2 \lambda_2^*}{\gamma_2 (\omega - \bar{u}_2^* k^*)^2} \sin(\lambda_2^* H_2) \cos(\lambda_1^* H_1) + \frac{\bar{a}_1^2 \lambda_1^*}{\gamma_1 (\omega - \bar{u}_1^* k^*)^2} \sin(\lambda_1^* H_1) \cos(\lambda_2^* H_2) = 0,$$
(2.14)

where

$$\lambda_1^{\color{red}*} = \left[ \frac{(\omega - \bar{u}_1^{\color{red}*} \, k^{\color{red}*})^2}{\bar{a}_1^2} - k^{\color{red}*2} \right]^{\frac{1}{2}}, \quad \lambda_2^{\color{red}*} = \left[ \frac{(\omega - \bar{u}_2^{\color{red}*} \, k^{\color{red}*})^2}{\bar{a}_2^2} - k^{\color{red}*2} \right]^{\frac{1}{2}}.$$

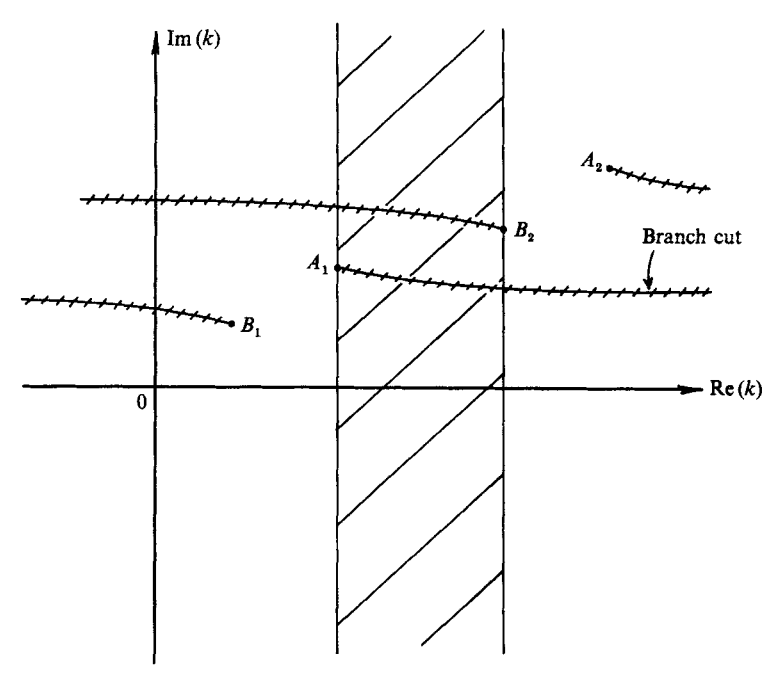


FIGURE 4. Complex k-plane showing branch-cut configuration of  $\lambda_1$  and  $\lambda_2$  for which supersonic instability is possible  $(\bar{u}_1 > \bar{u}_2)$ . Wavenumbers of supersonic instability waves are located in the shaded region.

## 2.3. Condition for the existence of supersonic instability waves

Consider first the case of two-dimensional disturbances (m = 0). The branch points of  $\lambda$  of (2.10) in the complex k-plane are (temporarily omitting the subscripts 1 and 2)

$$k_A = \frac{\omega}{\overline{u} - \overline{a}}, \quad k_B = \frac{\omega}{\overline{u} + \overline{a}}.$$
 (2.15)

Now in the discussion on the physical mechanism that leads to the existence of supersonic instability waves it is implicit that in the wave frame of reference the convective Mach numbers of the flows on the two sides of the shear layers must be supersonic. Suppose  $\bar{u}_1 > \bar{u}_2$ , then the phase velocity of an unstable shear wave would lie between these two values, namely,  $\bar{u}_1 > \text{Re}\left(\omega/k\right) > \bar{u}_2$ . In the complex k-plane it is readily shown that the condition for supersonic convective Mach number to exist on both sides of the shear layer is that the branch-cut configuration must be as shown in figure 4. In this figure the supersonic convective Mach number condition is satisfied by all the wavenumbers lying in the vertical strip between branch points  $A_1$  and  $B_2$ . Thus if one is interested only in the poles of the supersonic instability waves it is only necessary to locate the zeros of the dispersion function in this vertical strip. The condition that branch point  $B_2$  lies to the right of  $A_1$  is  $k_{B_2} > k_{A_1}(k_{A_2}, k_{B_1})$  are the wavenumbers of the branch points  $A_2$  and  $B_1$  respectively). This gives the condition for the existence of supersonic instability waves to be

$$\bar{u}_1 - \bar{u}_2 > \bar{a}_1 + \bar{a}_2. \tag{2.16}$$

For three-dimensional disturbances it is easy to find that the corresponding condition is

$$\frac{\overline{u}_2 - \overline{a}_2 [1 + (\overline{u}_2^2 - \overline{a}_2^2) (2m\pi)^2 / (\omega B)^2]^{\frac{1}{2}}}{\overline{u}_2^2 - \overline{a}_2^2} > \frac{\overline{u}_1 + \overline{a}_1 [1 + (\overline{u}_1^2 - \overline{a}_1^2) (2m\pi)^2 / (\omega B)^2]^{\frac{1}{2}}}{\overline{u}_1^2 - \overline{a}_1^2}. \quad (2.17)$$

For large m (with  $\omega$  fixed), inequality (2.17) cannot be satisfied, so that the higher-order three-dimensional modes are unable to exhibit supersonic instability. At low frequency,  $\omega \to 0$  (with  $m \neq 0$ ) inequality (2.17) again cannot be satisfied. Thus there is no low-frequency three-dimensional supersonic instability wave.

## 2.4. Finite-thickness shear-layer model

To account for finite shear-layer thickness effects a model with a velocity profile as illustrated in figure 3(b) will be used. For simplicity it will be assumed that the gases on the two sides of the mixing layer are inviscid, non-heat-conducting and non-reactive. Further, molecular diffusion processes, although present, will be neglected. Let  $C_1$  be the mass fraction of species 1 of the gas mixture. Since there are only two gas species it follows that the mass fraction of species 2 is equal to  $(1-C_1)$ . The continuity, momentum and energy equations of the gas mixture in the shear layer may be written in the form

$$\frac{\partial \rho}{\partial t} + \nabla \cdot (\rho v) = 0, \tag{2.18}$$

$$\rho\left(\frac{\partial \boldsymbol{v}}{\partial t} + \boldsymbol{v} \cdot \nabla \boldsymbol{v}\right) = -\nabla p, \tag{2.19}$$

$$\rho\left(\frac{\partial h}{\partial t} + \boldsymbol{v} \cdot \boldsymbol{\nabla} h\right) = \frac{\partial p}{\partial t} + \boldsymbol{v} \cdot \boldsymbol{\nabla} p, \qquad (2.20)$$

where  $\rho$ , v, p are the density, velocity and pressure of the gas mixture. h, the enthalpy of the gas mixture, is related to the temperature T and specific heats at constant pressure,  $C_{p_1}$  and  $C_{p_2}$ , of the gas components by

$$h = [C_{p_1}C_1 + C_{p_0}(1 - C_1)]T. (2.21)$$

The pressure of the gas mixture is equal to the sum of the partial pressures of the two gas components according to Dalton's law. This leads immediately to the equation of state for the gas mixture  $p = \rho RT, \qquad (2.22)$ 

where  $R = C_1 R_1 + (1 - C_1) R_2$ .  $R_1$  and  $R_2$  are the gas constants of the two gas components. The above equations do not form a complete set. They are to be supplemented by the species transport equation which, upon imposing the assumption of negligible diffusion, gives

$$\rho \left[ \frac{\partial C_1}{\partial t} + \boldsymbol{v} \cdot \boldsymbol{\nabla} C_1 \right] = 0. \tag{2.23}$$

The time-independent parallel-flow solution of the above system of equations is

$$\mathbf{v} = \bar{u}(y)\hat{e}_x, \quad C_1 = \bar{c}_1(y), \quad \rho = \bar{p}(y), \quad p = \bar{p} = \text{constant},$$
 (2.24)

where  $\bar{u}, \bar{c}_1, \bar{\rho}$  are arbitrary functions of y.

To find the instability characteristics of the shear layer inside a rectangular channel it is only necessary to solve the linearized form of (2.18)–(2.23). The linearization is to be carried out about the mean flow solution of (2.24). Let p(x, y, z, t) be the perturbation pressure associated with the small-amplitude disturbances superimposed on the mean flow. Under the locally parallel-flow approximation p may be taken to be of the form

$$p = \hat{p}(y) e^{i(kx - \omega t)} \cos(2m\pi z/B) \quad (m = 0, 1, 2, ...).$$
 (2.25)

Solution (2.25) automatically satisfies the boundary conditions at the two sidewalls  $z = \pm \frac{1}{2}B$ . Substituting (2.25) and other dependent variables of similar form into the linearized equations of motion and eliminating all other variables, it is found that the equation for  $\hat{p}(y)$  is

$$\frac{\mathrm{d}^2\hat{p}}{\mathrm{d}y^2} + \left[ \frac{2k}{(\omega - k\bar{u})} \frac{\mathrm{d}\bar{u}}{\mathrm{d}y} - \frac{1}{\bar{\rho}} \frac{\mathrm{d}\bar{\rho}}{\mathrm{d}y} \right] \frac{\mathrm{d}\hat{p}}{\mathrm{d}y} + \left[ \frac{(\omega - k\bar{u})^2}{\bar{a}^2} - k^2 - \left(\frac{2\pi m}{B}\right)^2 \right] \hat{p} = 0, \tag{2.26}$$

where  $\bar{a} = (\bar{\gamma}\bar{p}/\bar{p})^{\frac{1}{2}}$  is the speed of sound of the gas mixture.  $\bar{\gamma}$ , the ratio of the specific heats of the gas mixture, is

 $\bar{\gamma} = \frac{C_{p_1}C_1 + C_{p_2}(1-C_1)}{C_{v_*}C_1 + C_{v_2}(1-C_1)}.$ 

In the above expression  $C_{v_1}$  and  $C_{v_2}$  are the specific heats at constant volume of gas species 1 and 2 respectively. The solid surface boundary condition on the top and bottom walls of the channel requires

$$\frac{\mathrm{d}\hat{p}}{\mathrm{d}y} = 0 \quad \text{at} \quad y = H_1 \quad \text{and} \quad y = -H_2. \tag{2.27}$$

Outside the shear layer, i.e.  $y > \delta$  or  $y < -\delta$ , the flow is uniform so that the second term of (2.26) vanishes. The solution of this equation that satisfies boundary condition (2.27) is

$$\overline{p} = E \cos \left[ \lambda_1 (H_1 - y) \right] \quad (H_1 \geqslant y \geqslant \delta), \tag{2.28}$$

$$p = F \cos\left[\lambda_2(y + H_2)\right] \quad (-\delta \geqslant y \geqslant -H_2),\tag{2.29}$$

where  $\lambda_1$  and  $\lambda_2$  are given by (2.10) and E and F are arbitrary constants. To find the solution of (2.26) inside the shear layer one may use (2.29) as a starting solution and integrate the equation numerically from  $y = -\delta$  until  $y = \delta$  is reached. Let the numerical solution be Ff(y). At  $y = \delta$  this solution must match that of (2.28). The continuity of  $\hat{p}$  and its derivative leads to the following equations:

$$\begin{split} E\cos\left[\lambda_1(H_1-\delta)\right] - Ff(\delta) &= 0,\\ \lambda_1 E\sin\left[\lambda_1(H_1-\delta)\right] - Ff'(\delta) &= 0. \end{split}$$

For non-trivial solution of the unknowns E and F the determinant of the coefficient matrix D must be equal to zero. This yields the eigenvalue equation

$$D \equiv -\cos{[\lambda_1(H_1-\delta)]}f'(\delta) + \lambda_1\sin{[\lambda_1(H_1-\delta)]}f(\delta) = 0. \tag{2.30} \label{eq:2.30}$$

In general, D is not equal to zero unless for a given  $\omega, k$  takes on special values (eigenvalues). To determine k, Newton's iteration method may be applied to (2.30). As a starting value in the iteration process the value of k obtained by the vortex-sheet model may be used.

## 3. Computation procedure and pole merging phenomenon

To describe the general motion of a supersonic shear layer inside a rectangular channel infinitely many normal modes are needed. If a vortex-sheet model is used to represent the shear layer, these normal modes are given by the zeros (or poles) of the dispersion function  $D(\omega, k)$  of (2.12). In this paper an effort will be made to classify these wave modes (both neutrally stable and unstable) into families according to their physical and mathematical properties. Since the number of wave modes

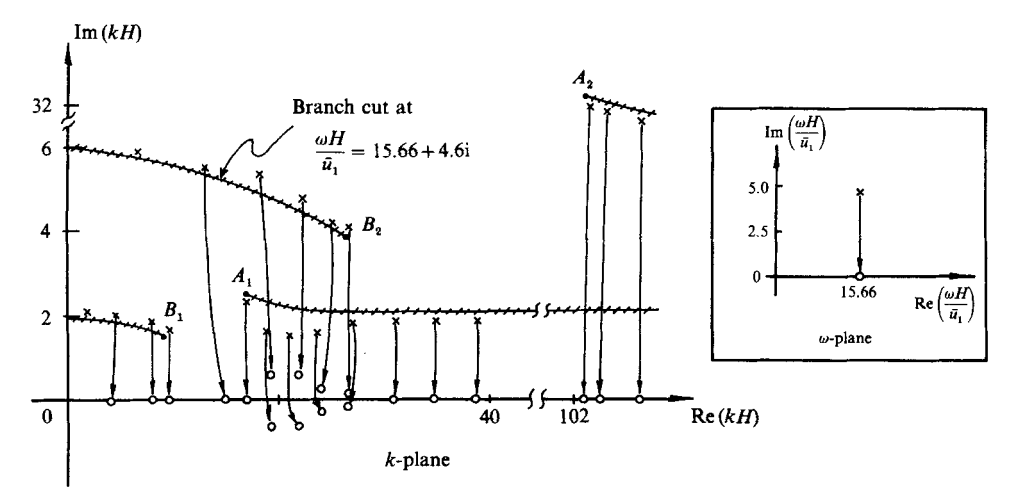


FIGURE 5. Trajectories of the poles or zeroes of  $D(\omega, k)$  as the  $\omega$ -contour is pushed toward the real axis following the Briggs' criterion.  $M_1 = 3.4(\text{He}), M_2 = 1.6(\text{N}_2), H_1 = H_2, \bar{\alpha}_1/\bar{\alpha}_2 = 1.63.$ 

considered is very large an efficient way of determining the zeros of  $D(\omega, k)$  for a prescribed complex or real value of  $\omega$  is needed. In the present investigation this is done by means of a grid-search procedure.

The dispersion function,  $D(\omega, k)$ , of (2.12) involves only elementary trigonometric functions, so the numerical value of the function can be easily calculated. To implement the grid-search technique a finite region of the complex k-plane in which the normal modes are to be determined is first selected. This region is then subdivided into smaller regions by a rectangular grid. The values of  $D(\omega, k)$  at each grid point are calculated. A contour subroutine which is capable of using this set of values to determine and to draw the curves Re(D) = 0 and Im(D) = 0 in the k-plane by two-dimensional interpolation is called. The intersection of these two families of curves are the approximate roots of the dispersion function. To refine the values of the roots or poles Newton's iteration method is used.

In this work the primary interest is the spatial instability wave modes. For spatial instability waves  $\omega$  is real. However, it is known that in determining these waves it is not sufficient to set  $\omega$  to a real number and look for the zeros or poles of D in the complex k-plane. One must recognize that waves can propagate in the positive or negative x-direction. Such a distinction is absolutely necessary. Failure to do so may erroneously treat an evanescent wave as a spatially growing wave and vice versa. Here the criterion for distinguishing between an evanescent and a spatially amplifying wave established by Briggs (1964) will be followed. According to Briggs, if one is interested in spatial instability waves of frequency  $\Omega$  one should start calculating the roots or poles of the dispersion function by setting the real part of  $\omega$  equal to  $\Omega$  and the imaginary part of  $\omega$  to be a large positive value. Zeros or poles of D lying in the upper half-k-plane represent wave propagating in the positive x-direction while those in the lower half-k-plane represent waves propagating in the negative x-direction. Figure 5 shows a typical example. For this case, the parameters of the mean flow have been taken to be:

Fluid 1; Helium,  $M_1 = 3.4$ ,  $\gamma_1 = \frac{5}{3}$ . Fluid 2; Nitrogen,  $M_2 = 1.6$ ,  $\gamma_2 = \frac{2}{5}$ .

$$H_1 = H_2$$
,  $\bar{a}_1/\bar{a}_2 = 1.63$ ,  $\bar{u}_1/\bar{u}_2 = 3.46$ .

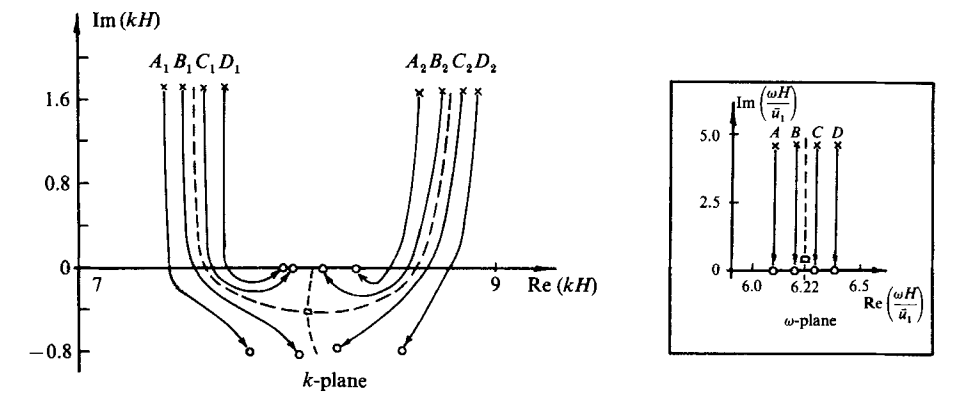


FIGURE 6. Trajectories of a pair of poles in the k-plane showing pole merging phenomenon.

With  $\omega H/\bar{u}_1 = 15.66 + 4.6i$  the poles of D are located in the k-plane by the gridsearch procedure described above. In figure 5 these poles are denoted by crosses. Also shown in this figure are the branch cuts of  $\lambda_1$  and  $\lambda_2$ . Now to obtain the normal mode solutions the point  $\omega$  must be pushed towards the real axis with real  $\omega$  kept fixed in the complex  $\omega$ -plane. Numerically this is carried out by reducing the imaginary part of  $\omega$  by small increments until it is equal to zero. For each intermediate value of  $\omega$ the grid-search procedure is implemented. In this way the movement of all the poles or zeros of  $D(\omega, k)$  can be traced during this  $\omega$ -contour deformation process. The trajectories of the poles are shown in figure 5. Some of the poles in the vertical strip between branch points  $A_1$  and  $B_2$  crossed into the lower half-k-plane as  $\omega$  is pushed toward the real axis. These are the supersonic instability wave modes. In figure 5 the positions of the poles in the k-plane corresponding to  $\omega$  on the real axis of the  $\omega$ -plane are denoted by small circles. They are the normal modes of the flow. In addition to the supersonic instability wave modes there are two families of poles lying on the real k-axis; one to the left of branch point  $A_1$ , the other to the right of branch point  $B_2$ . These are the neutral acoustic wave modes. Some poles remain in the upper halfk-plane. They represent spatial evanescent waves. It is to be noted that all the poles of the dispersion function originated from the upper half-k-plane so that the supersonic instability waves are convectively unstable and all the waves propagate in the downstream direction.

In the course of performing the  $\omega$ -contour deformation process according to Briggs' criterion, a pole merging phenomenon was observed. This occurs when special values of  $\Omega$  are chosen. When Re ( $\omega$ ) is set equal to one of these special values, two neighbouring poles would merge during the  $\omega$ -contour deformation process. An example is shown in figure 6 at  $\Omega H/\bar{u}_1=6.22$ . The trajectories of the two neighbouring poles in the range  $7.0 \leq \mathrm{Re}\,(kH) \leq 9.0$  and  $6.0 \leq \mathrm{Re}\,(\omega H/\bar{u}_1) \leq 6.5$  are plotted in this figure. The trajectories exhibit a saddle configuration. For the special case of  $\mathrm{Re}\,(\omega H/\bar{u}_1)=6.22$  the two poles first approach each other as  $\mathrm{Im}\,(\omega H/\bar{u}_1)$  is reduced. They merge, split apart and then move in opposite directions. Now it is important to point out that the observed pole merging phenomenon does not imply absolute instability. This is because both poles originated from the same side of the k-plane so that pole pinching, a necessary condition for absolute instability (see Briggs 1964), does not occur. In the present case the  $\omega$ -contour can be pushed all the way to the real axis without any difficulty. Therefore, no special treatment is needed in calculating the contributions of the two poles.

In classifying wave modes it is a usual practice to associate a wave mode with a particular pole in the k-plane. However, with pole merging, such an identification scheme would lead to discontinuities in the  $k=k(\omega)$  relationship and, perhaps, even confusion. To see this, consider the poles in figure 6 as  $\omega$  (real) increases. For  $\omega H/\bar{u}_1 < 6.22$ , the first pole denoted by trajectories  $A_1$  and  $B_1$  is an unstable pole with  $k_i < 0$ . However, for  $\omega H/\bar{u}_1 > 6.22$  this pole, now having trajectories  $C_1$  and  $D_1$  which terminate on the real k-axis, represents a neutral acoustic wave. Clearly an apparent discontinuity takes place at  $\omega H/\bar{u}_1 = 6.22$ . On the other hand the second pole with trajectories  $A_2, B_2, C_2$  and  $D_2$  also exhibits a similar discontinuity. But the nature of the discontinuity is exactly opposite to that of the first pole. Now if the poles are not singled out individually but are considered as a pair simultaneously then there is always a neutral wave mode and an unstable mode with no discontinuous behaviour as  $\omega H/\bar{u}_1$  varies. This is so even across the value 6.22. The point here is that merged poles have lost their individual identity. Both poles must be taken into consideration at the same time. When the poles are treated in this way no confusion can arise.

#### 4. Numerical results

As an illustration of the properties of supersonic instability waves associated with a two-dimensional shear layer inside a rectangular channel, the case of a supersonic mixing layer formed by helium (region 1) on one side and nitrogen (region 2) on the other will be discussed here. The mean flow conditions in this case study are

$$\begin{split} M_1 = 4.5, \quad M_2 = 1.6, \quad H_1 = H_2, \quad \bar{a}_1/\bar{a}_2 = 1.29, \\ \gamma_1 = \frac{5}{3}, \quad \gamma_2 = \frac{7}{5}, \quad H = B \text{ (for three-dimensional waves)}. \end{split}$$

Under these highly supersonic mean flow conditions it is easy to show that for a thin vortex-sheet shear layer in an unconfined environment, the familiar two-dimensional Kelvin–Helmholtz wave is neutrally stable (see Miles 1958). Thus the two-dimensional instability wave modes obtained in the present calculation are not related to the Kelvin–Helmholtz instability. They are new instability waves generated by the coupling of the motion of the shear layer and the acoustic modes (reflections) of the rectangular channel. It will be shown later that for shear layers with finite thickness the first two-dimensional mode of the new instability waves has the highest spatial growth rate.

Reflections by the surrounding walls on the coupled disturbances involving the acoustic modes of the channel and the oscillatory motion of the shear layer produce several families of instability and neutral waves. Numerical solutions of the dispersion function (2.12) indicate that there are basically four families of wave modes; two being unstable and two neutral. They will be referred to as class A, B, C and D waves. For clarity, each mode of a wave family will be designated by two integer numbers (m,n): n is the transverse mode number primarily related to reflections from the top or bottom wall of the rectangular channel; m is the lateral mode number related to reflections from the two sidewalls. Thus within each class or family of waves the modes are labelled as  $A_{mn}, B_{mn}, C_{mn}$  and  $D_{mn}(m=0,1,2,\ldots; n=1,2,3,\ldots)$  respectively.

## 4.1. Results of vortex-sheet model

In this subsection the two-dimensional wave modes (m = 0) will first be examined. Numerical solutions of the dispersion function (2.12) for spatial instability following

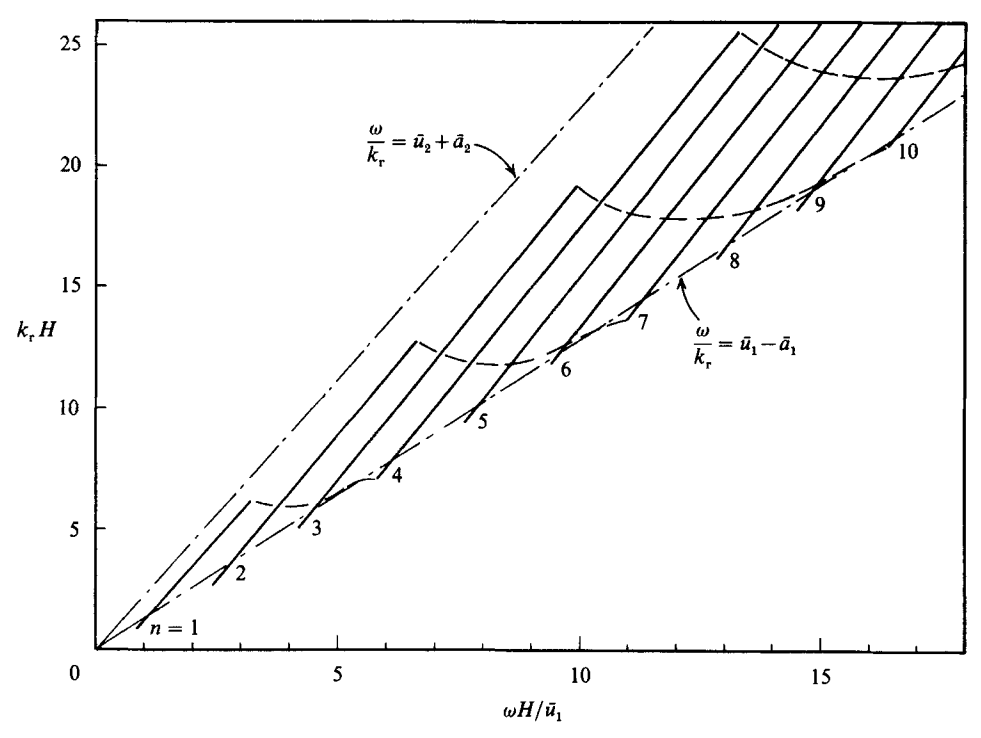


Figure 7. Dispersion relation of class A supersonic instability waves.  $M_1=4.5({\rm He}),$   $M_2=1.6({\rm N}_2),\,H_1=H_2,\,\bar{a}_1/a_2=1.29.$  instability wave, ---- neutral wave, m=0.

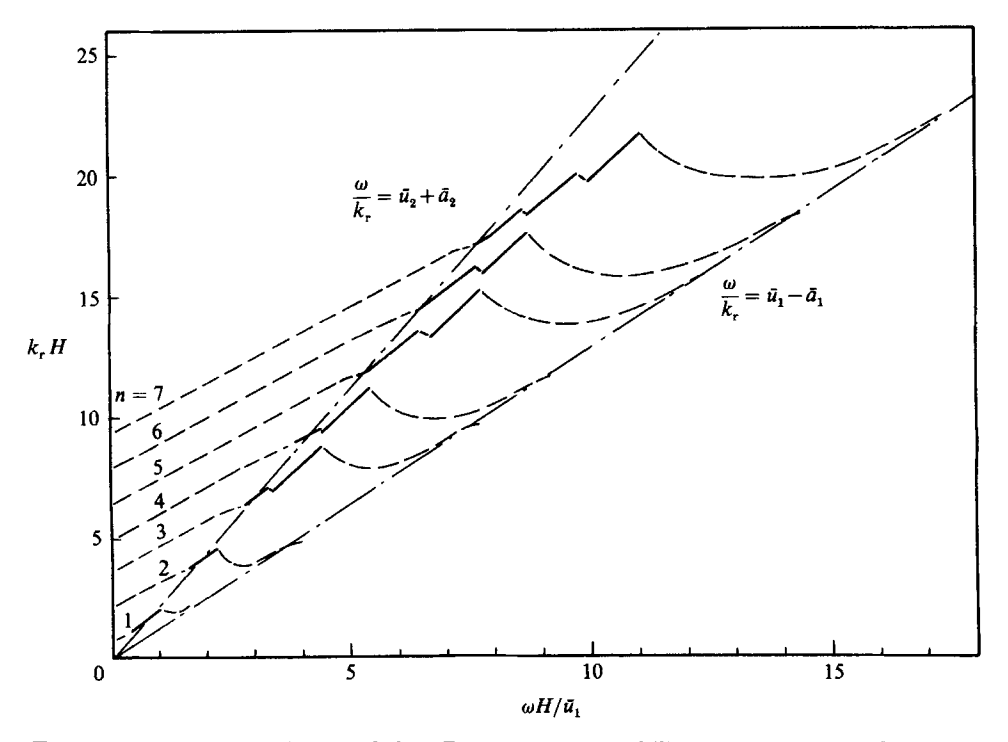


Figure 8. Dispersion relation of class B supersonic instability waves (----) and class C neutral acoustic waves (-----).  $M_1=4.5({\rm He}),\,M_2=1.6({\rm N_2}),\,H_1=H_2,\,\bar{\alpha}_1/\bar{\alpha}_2=1.29,\,m=0.$ 

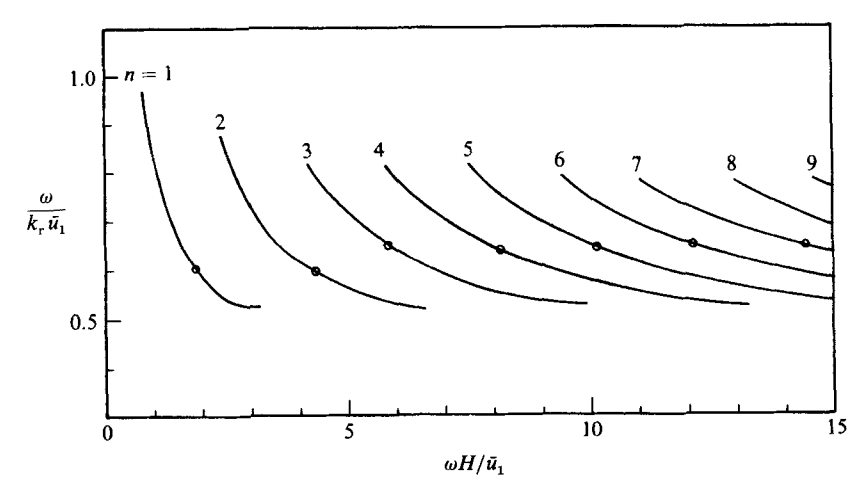


FIGURE 9. Phase velocity of class A supersonic instability waves.  $M_1 = 4.5$ (He),  $M_2 = 1.6$ (N<sub>2</sub>),  $H_1 = H_2$ ,  $\bar{a}_1/\bar{a}_2 = 1.29$ , m = 0.  $\bigcirc$ , Wave with maximum growth rate.

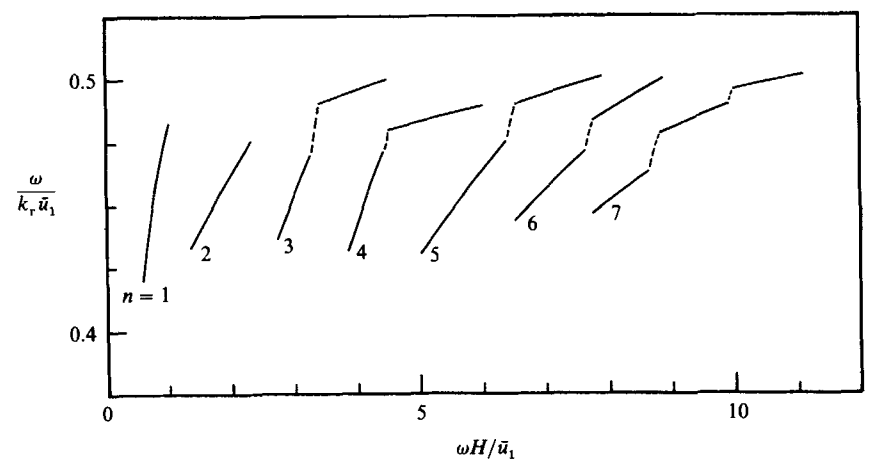


Figure 10. Phase velocity of class B supersonic instability waves.  $M_1=4.5({\rm He}),~M_2=1.6({\rm N_2}),~H_1=H_2,~\bar{a}_1/\bar{a}_2=1.29,~m=0.$ 

the Briggs' (1964) procedure shows that the flow is convectively unstable. There are basically two families of supersonic instability wave modes. They will be referred to as class A and class B modes. The dispersion relations (real part of the wavenumber as a function of frequency) of these waves are given in figures 7 and 8. Since these unstable waves exist only when the convective Mach numbers are supersonic they can be found only in the sector

$$\overline{u}_2 + \overline{a}_2 \leqslant \frac{\omega}{k_r} \leqslant \overline{u}_1 - \overline{a}_1$$

of the  $(\omega, k_r)$  plane. The phase velocities of the class A supersonic instability waves generally decrease as the wave frequency increases. This is shown in figure 9. On the other hand, the phase velocities of class B supersonic instability waves behave differently. They increase with frequency as illustrated in figure 10. Figure 11 shows the growth rate of the class A instability wave modes. For a given mode the wave is

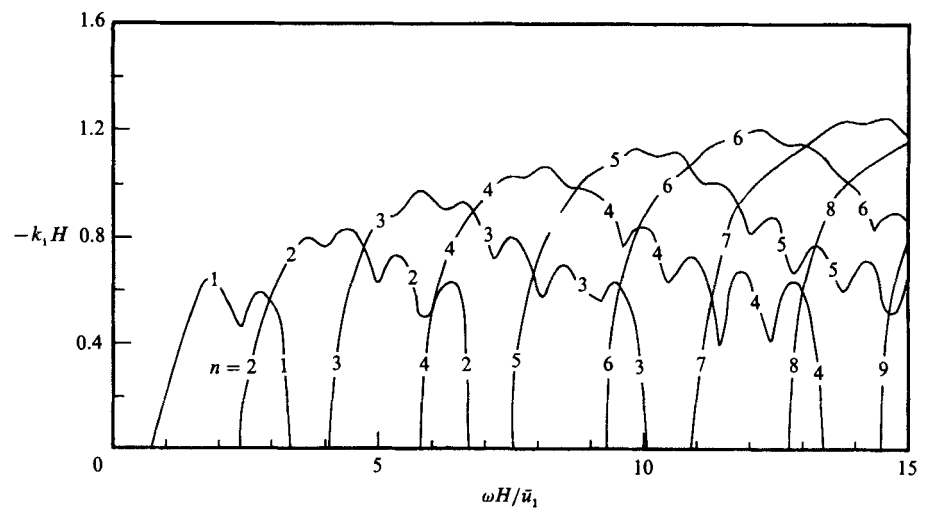


Figure 11. Spatial growth rate of class A supersonic instability waves.  $M_1=4.5({\rm He}),$   $M_2=1.6({\rm N_2}),$   $\bar{a}_1/\bar{a}_2=1.29,$   $H_1=H_2,$  m=0.

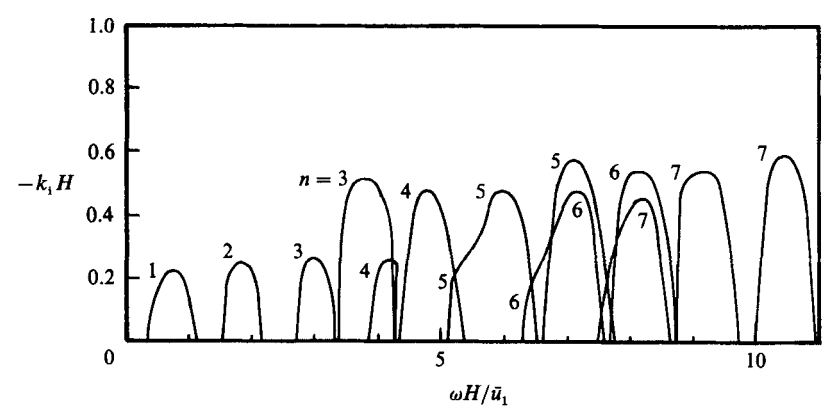


Figure 12. Spatial growth rate of class B supersonic instability waves.  $M_1=4.5({\rm He}),$   $M_2=1.6({\rm N_2}),$   $\bar{a}_1/\bar{a}_2=1.29,$   $H_1=H_2,$  m=0.

unstable only over a finite frequency band. But collectively there is at least one, and often more than one, unstable wave mode for a given frequency. Figure 12 provides the growth rate of the class B instability waves. For the chosen mean flow conditions, class B waves have smaller growth rates than their class A counterparts. Hence it appears that they are less important.

For thin shear layers, typical pressure distributions (eigenfunctions) associated with class A supersonic instability waves are given in figure 13. These eigenfunctions are characterized by oscillations in the direction normal to the mean flow. These oscillations are characteristic features of standing wave patterns. Roughly speaking, they indicate the number of nodes and antinodes resulting from acoustic reflections from the channel walls. Figure 14 shows similar eigenfunctions of class B supersonic instability waves at the maximum growth rate. Unlike the eigenfunctions in figure 13, which have standing wave patterns primarily in the region below the shear layer (region 2), they exhibit oscillations mainly in the region above the shear layer.

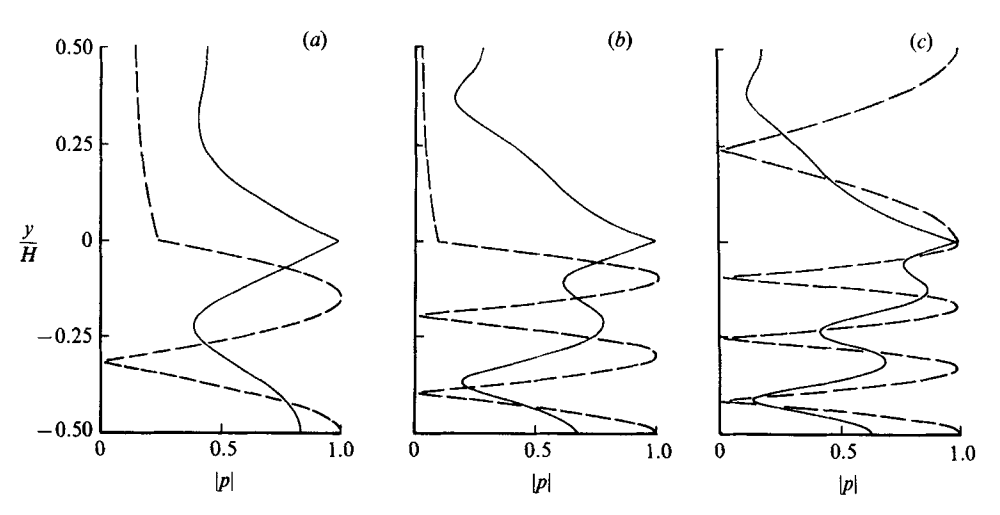


FIGURE 13. Eigenfunctions (pressure) of class A supersonic instability waves at maximum growth rate and class D neutral acoustic waves. (a) ——, Mode  $A_{01}$ ,  $\omega H/\bar{u}_1 = 1.8$ , kH = 2.943-0.645i; ——, Mode  $D_{01}$ ,  $\omega H/\bar{u}_1 = 2.25$ , kH = 2.4. (b) ——, Mode  $A_{02}$ ,  $\omega H/\bar{u}_1 = 4.2$ , kH = 6.940-0.838i; ——, Mode  $D_{02}$ ,  $\omega H/\bar{u}_1 = 3.95$ , kH = 4.3. (c) ——, Mode  $A_{03}$ ,  $\omega H/\bar{u}_1 = 5.8$ , kH = 8.978-0.974i; ——, Mode  $D_{03}$ ,  $\omega H/\bar{u}_1 = 4.0$ , kH = 2.52.

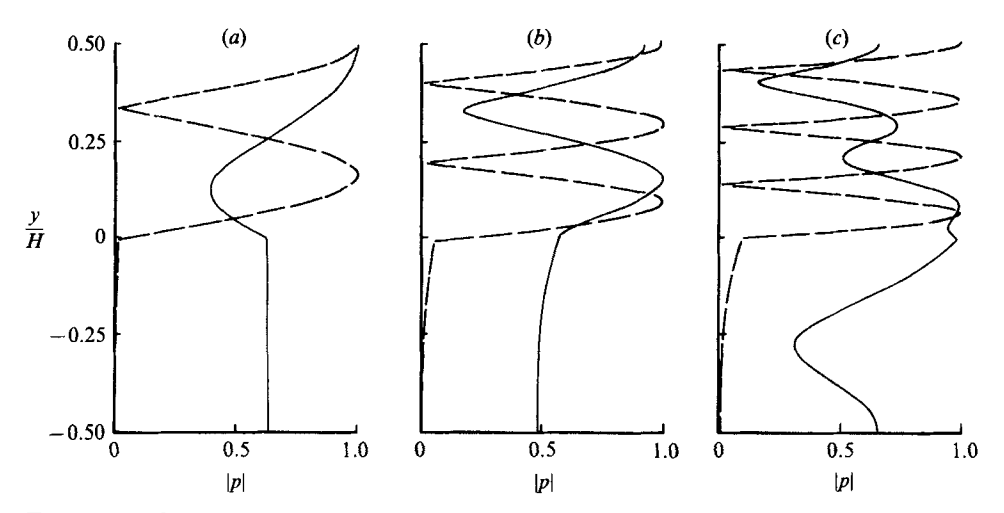


FIGURE 14. Eigenfunctions (pressure) of class B supersonic instability waves at maximum growth rate and class C neutral acoustic waves. (a) ——, Mode  $B_{01}$ ,  $\omega H/\bar{u}_1 = 0.80$ , kH = 1.751-0.218; ——, Mode  $C_{02}$ ,  $\omega H/\bar{u}_1 = 1.0$ , kH = 3.207. (b) ——, Mode  $B_{03}$ ,  $\omega H/\bar{u}_1 = 1.80$ , kH = 4.038-0.257i; ——, Mode  $C_{03}$ ,  $\omega H/\bar{u}_1 = 2.0$ , kH = 5.687. (c) ——, Mode  $B_{03}$ ,  $\omega H/\bar{u}_1 = 3.8$ , kH = 7.697-0.528i, ——, Mode  $C_{04}$ ,  $\omega H/\bar{u}_1 = 3.0$ , kH = 8.174.

Obviously these two classes of waves are formed by reflections principally from either the top or the bottom wall of the channel.

In addition to the two classes of supersonic instability waves there are basically two families of neutral acoustic waves. These neutral acoustic modes are not unrelated to the instability waves modes. The dispersion relations (i.e.  $k = k(\omega)$ ) of the first family of neutral acoustic modes (referred to as class C modes) are given (dotted curves) in figure 8. As frequency increases these neutral acoustic waves evolve into class B supersonic instability waves. The real part of the wavenumber of

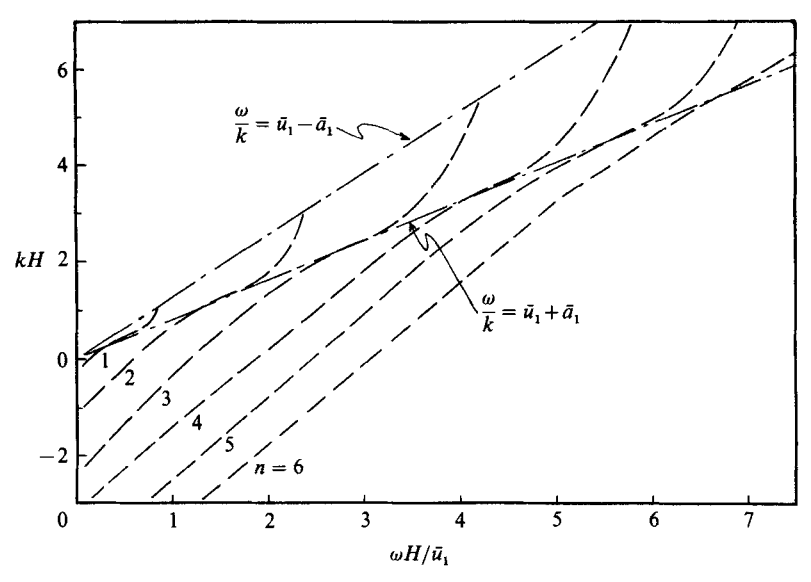


Figure 15. Dispersion relation of class D neutral wave modes (---).  $M_1=4.5({
m He}),$   $M_2=1.6({
m N_2}),~H_1=H_2,~\bar{a}_1/\bar{a}_2=1.29,~m=0.$ 

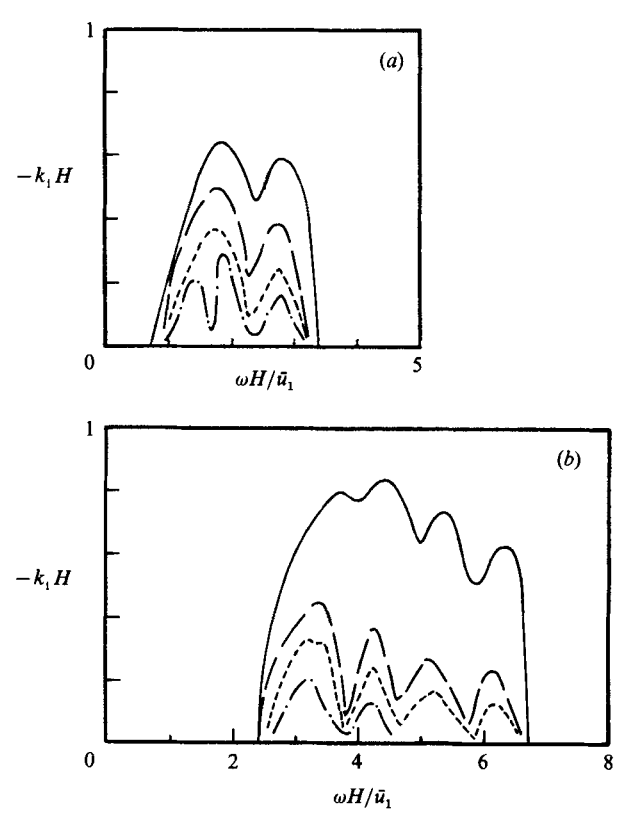


Figure 16. Effect of finite shear-layer thickness on the growth rate of class A supersonic instability waves.  $M_1=4.5(\mathrm{He}),~M_2=1.6(\mathrm{N_2}),~H_1=H_2,~\bar{a}_1/\bar{a}_2=1.29.$  —,  $\delta_\omega/H=0$ ; —--,  $\delta_\omega/H=0.05$ ; —---,  $\delta_\omega/H=0.15$ . (a) Mode  $A_{01}$ ; (b) mode  $A_{02}$ .

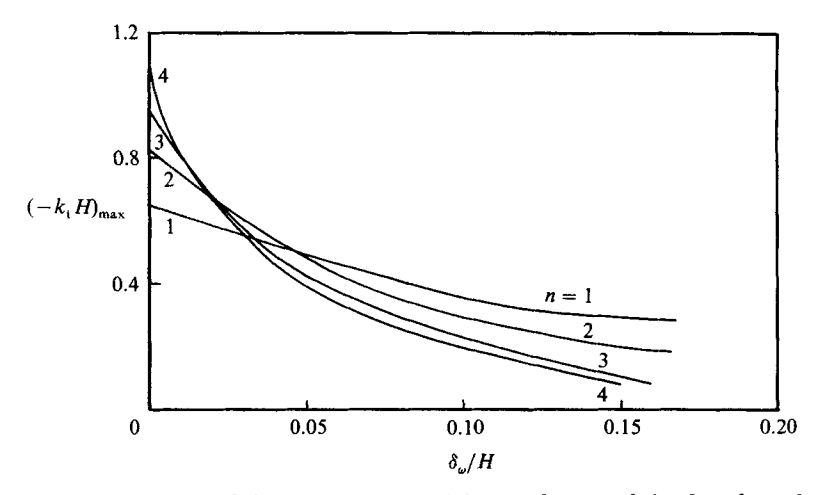


FIGURE 17. Dependence of the maximum spatial growth rate of the first four class A supersonic instability wave modes on vorticity thickness of the shear layer. m = 0,  $M_1 = 4.5$ (He),  $M_2 = 1.6$ (N<sub>2</sub>).

the neutral C mode and that of the unstable B mode form a continuous function of the wave frequency, while the imaginary part of the wavenumber is zero for the neutral wave and negative for the unstable wave. The dispersion relations of the second family (class D) of neutral acoustic waves are shown in figure 15. Typical wave patterns or eigenfunctions of these waves are provided in figures 13 and 14. They form standing wave patterns characteristic of normal acoustic modes inside a duct. As in the case of supersonic instability waves, all the neutral acoustic waves propagate in the downstream direction. This is to be expected since the flows on both sides of the shear layer are supersonic.

## 4.2. Results of finite-thickness shear-layer model

The effect of finite shear-layer thickness has been investigated using the flow model described in §2.4. In the present computations the mean velocity and concentration profiles are assumed to be in the shape of hyperbolic tangent functions. Specifically, the following mean flow profiles are adopted:

$$\begin{split} \overline{u}(y) &= \tfrac{1}{2} [\overline{u}_1 + \overline{u}_2 + (\overline{u}_1 - \overline{u}_2) \tanh{(2y/\delta_\omega)}], \\ \overline{c}_1(y) &= \tfrac{1}{2} [1 + \tanh{(2y/\delta_\omega)}], \end{split}$$

where  $\delta_{\omega}$  is the vorticity thickness of the shear layer. The mean density  $\bar{\rho}$  is obtained by the Crocco's relation. The total temperatures of both streams adjacent to the shear layer are not assumed to be the same. Figure 16 shows the change in growth rate of the first two modes of class A waves as a function of the vorticity thickness of the shear layer. As the shear layer becomes thicker and thicker, at a fixed frequency, the growth rate of the supersonic instability waves decreases. The same is true for class B instability waves. Figure 17 gives the dependence of the maximum spatial growth rates of supersonic instability wave modes  $A_{01}, A_{02}, A_{03}$ , and  $A_{04}$  on the vorticity thickness of the shear layer. Of importance is the observation that, while for very thin shear layers the maximum growth rates of the lower-order modes are smaller than those of the higher-order modes, the reverse is true for thicker shear layers. In practical situations it is expected that the  $A_{01}$  mode is most dominant.

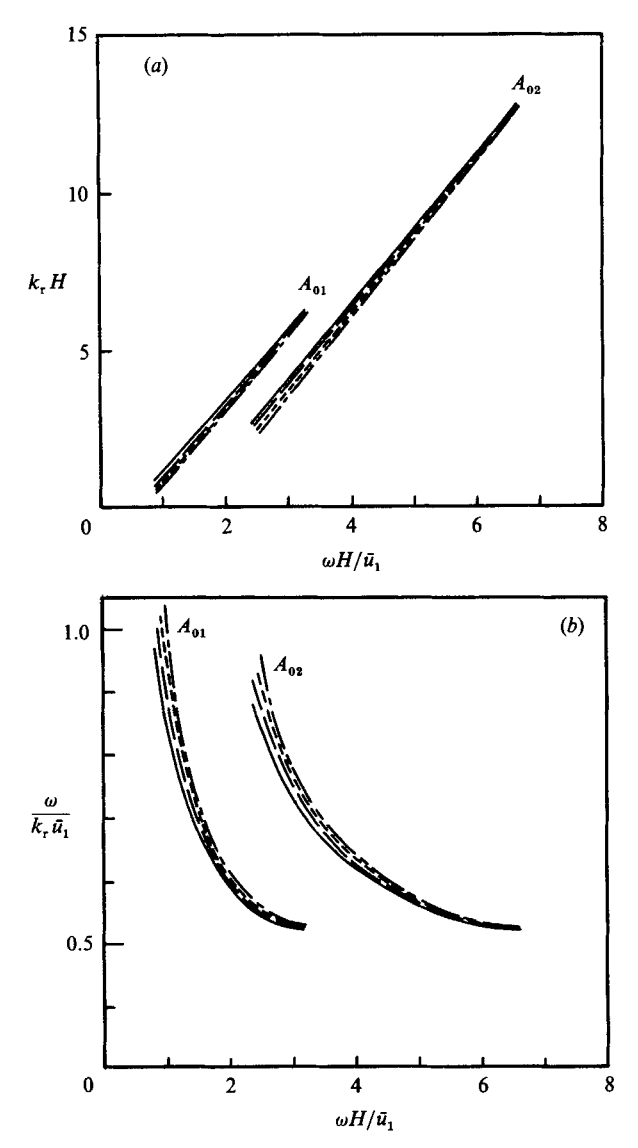


FIGURE 18. Effect of finite shear-layer thickness on (a) the wavenumber and (b) the phase velocity of class A supersonic instability waves.  $M_1 = 4.5 (\text{He})$ ,  $M_2 = 1.6 (\text{N}_2)$ ,  $H_1 = H_2$ ,  $\bar{\alpha}_1/\bar{\alpha}_2 = 1.29$ . —,  $\delta_{\omega}/H = 0$ ; ——,  $\delta_{\omega}/H = 0.1$ ; ——,  $\delta_{\omega}/H = 0.15$ .

Figure 18 shows the effect of shear-layer thickness on the dispersion relations and the phase velocities of the class A supersonic instability waves. It is clear from these results that the phase velocities are only slightly affected by the finite-thickness effect. The same is true for class B supersonic instability waves. On the other hand, shear-layer thickness does have a profound effect on the growth rate of these waves. This is illustrated in figure 19. At a reasonable shear layer thickness, the growth rates of class B instability waves are so greatly reduced that they may, for all intents and purposes, be regarded as neutral waves.

The eigenfunctions of the most unstable  $A_{01}$  supersonic instability waves at different shear-layer thicknesses are given in figure 20. On comparing these figures

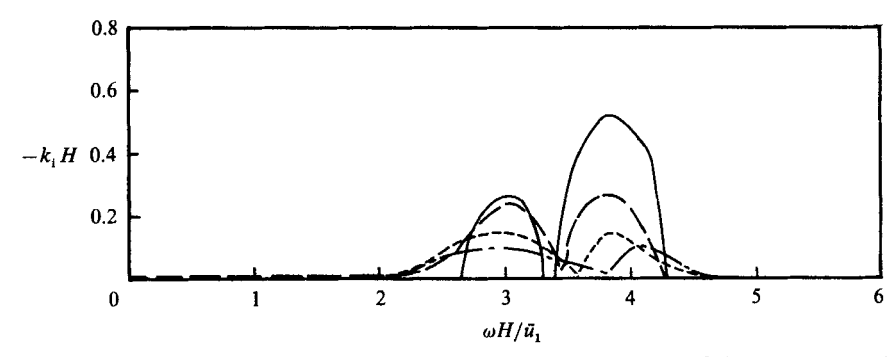


FIGURE 19. Effect of finite shear-layer thickness on the growth rate of class B supersonic instability waves.  $M_1 = 4.5$ (He),  $M_2 = 1.6$ (N<sub>2</sub>),  $H_1 = H_2$ ,  $\bar{\alpha}_1/\bar{\alpha}_2 = 1.29$ , Mode  $B_{03}$ . ——,  $\delta_{\omega}/H = 0$ ; ——,  $\delta_{\omega}/H = 0.1$ ; ———,  $\delta_{\omega}/H = 0.15$ .

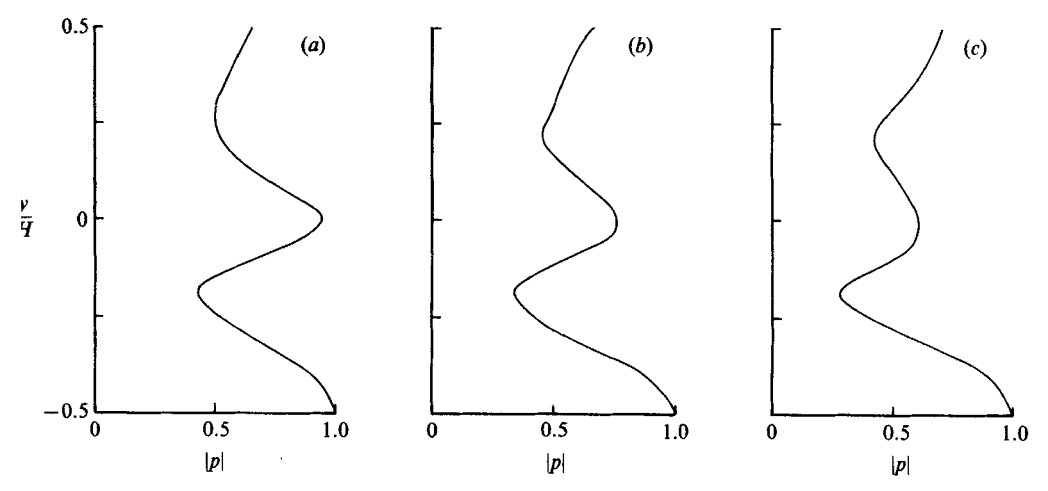


FIGURE 20. Effect of finite shear-layer thickness on the eigenfunction of  $A_{01}$  supersonic instability wave mode. Shown are waves at maximum growth rate.  $M_1=4.5({\rm He}),\,M_2=1.6({\rm N_2}).\,(a)\,\,\delta_\omega/H=0.05,\,\omega H/\bar{u}_1=1.8,\,kH=2.972-0.510i.\,(b)\,\,\delta_\omega/H=0.1,\,\omega H/\bar{u}_1=1.8,\,kH=2.982-0.426i.\,(c)\,\,\delta_\omega/H=0.15,\,\omega H/\bar{u}_1=1.8,\,kH=2.975-0.357i.$ 

with figure 13(a), which corresponds to the case of zero thickness, it is evident that there is no qualitative difference. The effect of using a continuous velocity profile shear-layer model is to smooth out the apparent discontinuity in the slope of the eigenfunction of the vortex-sheet model. The above remarks are also applicable to the higher-order modes and to class B supersonic instability waves.

## 4.3. Three-dimensional wave modes

Owing to reflections from the two sidewalls a shear layer inside a rectangular channel is also subjected to three-dimensional instabilities. In the present investigation these three-dimensional instability modes have been studied using both the vortex-sheet and the finite-thickness shear-layer models. Generally speaking, the characteristics of the three-dimensional instability wave modes are found to be similar to those of the corresponding two-dimensional modes. For shear layers that are reasonably thick numerical results indicate that the class A two-dimensional supersonic instability waves have larger spatial growth rates than their three-dimensional counterparts.

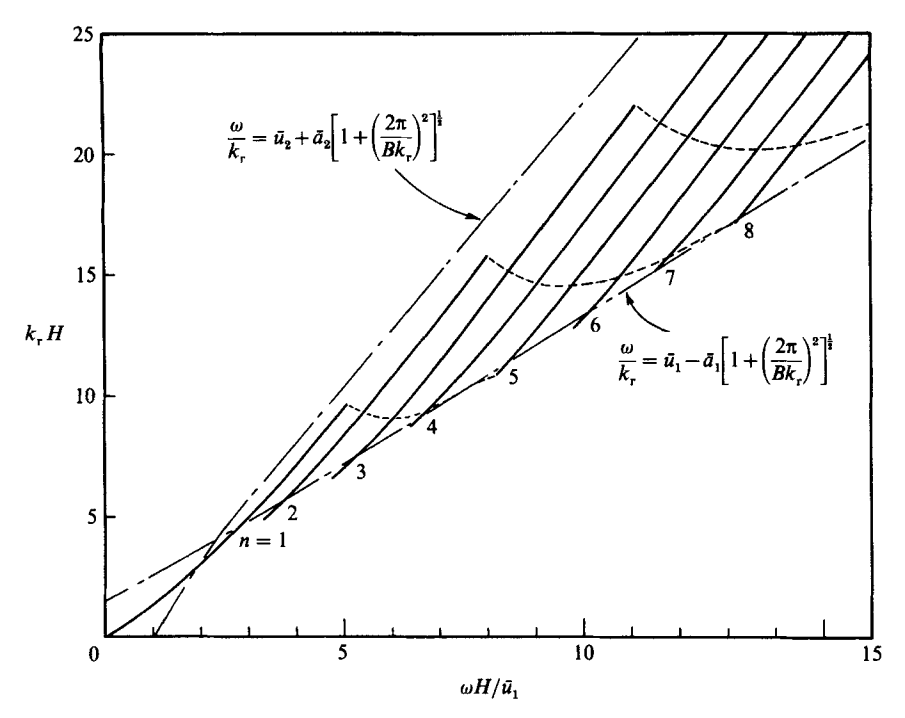


FIGURE 21. Dispersion relation of three-dimensional class A supersonic instability waves.  $M_1=4.5({\rm He}),~M_2=1.6({\rm N_2}),~H_1=H_2=\frac{1}{2}B,~\bar{a}_1/\bar{a}_2=1.29,~m=1,~\delta_\omega=0.$  instability wave; ...., neutral wave.

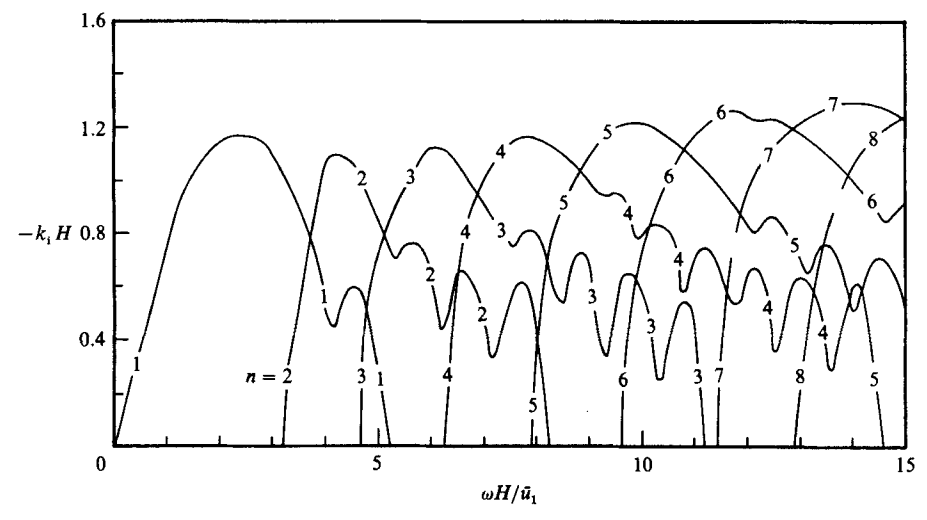


Figure 22. Spatial growth rate of three-dimensional class A supersonic instability waves.  $M_1=4.5 ({\rm He}),\, M_2=1.6 ({\rm N_2}),\, H_1=H_2=\frac{1}{2}B,\, \bar{a}_1/\bar{a}_1=1.29,\, m=1,\, \delta_\omega=0.$ 

Thus experimentally the most likely observable wave belongs to the  $A_{01}$  mode, the lowest-order two-dimensional instability wave mode.

Figure 21 shows the dispersion relations of the m=1 three-dimensional class A instability waves. Except at the very low-Strouhal-number range, qualitatively the characteristics of these dispersion relations are the same as those given in figure 7.

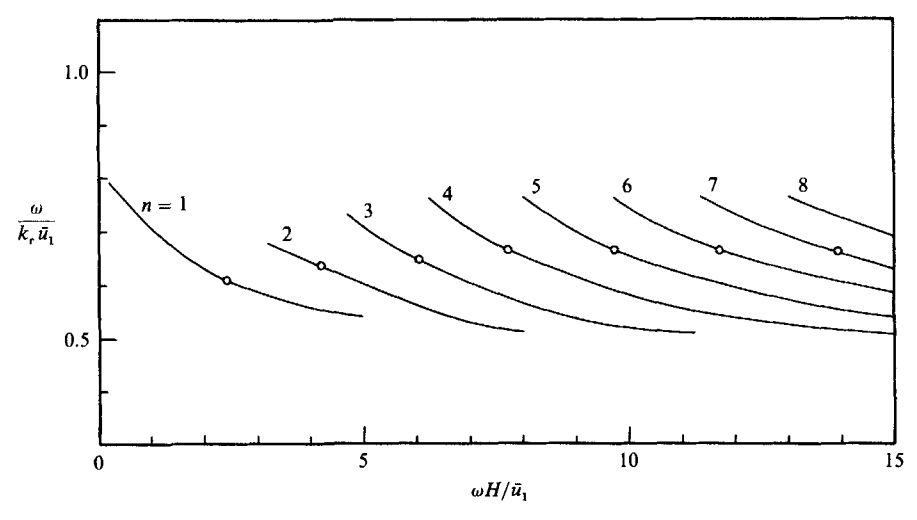


FIGURE 23. Phase velocity of three-dimensional class A supersonic instability waves.  $M_1=4.5({\rm He}),$   $M_2=1.6({\rm N_2}),$   $H_1=H_2=\frac{1}{2}B,$   $\overline{a}_1/\overline{a}_2=1.29,$  m=1,  $\delta_\omega=0.$   $\bigcirc$ , Wave with maximum growth rate.

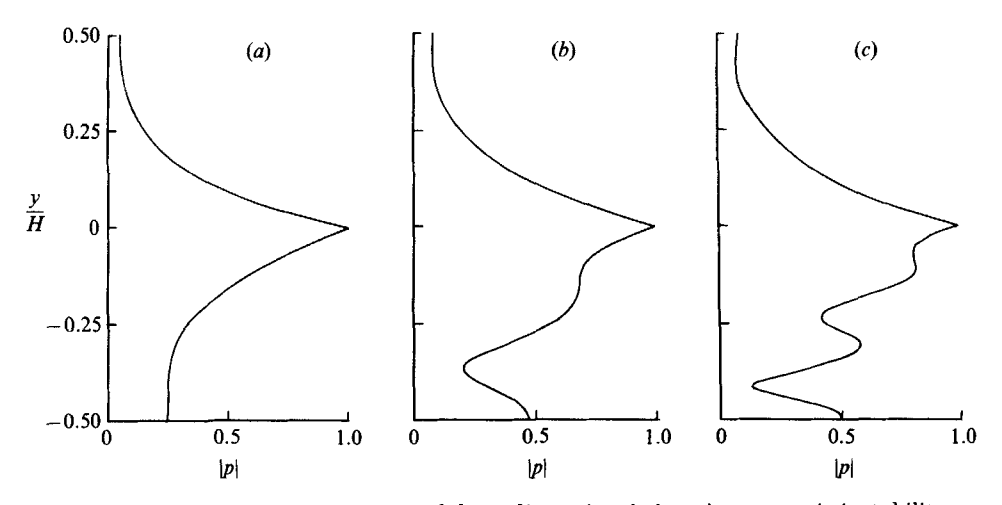


Figure 24. Eigenfuctions (pressure) of three-dimensional class A supersonic instability waves at maximum growth rate.  $\delta_{\omega}=0$ . (a) Mode  $A_{11}$ ,  $\omega H/\bar{u}_1=2.39$ , kH=3.863-1.187i. (b) Mode  $A_{12}$ ,  $\omega H/\bar{u}_1=4.18$ , kH=6.532-1.089i. (c) Mode  $A_{13}$ ,  $\omega H/\bar{u}_1=5.97$ , kH=9.106-1.134i.

The same is true for class B instability waves. The growth rates of class A instability waves are shown in figure 22. Again it is found that class A supersonic instability waves have significantly higher growth rates than class B waves. They are, therefore, expected to be the dominant wave modes. It is interesting to point out that unlike the two-dimensional waves (m=0) the maximum growth rate of the lowest-order mode,  $A_{11}$ , is not small. In fact, its maximum value is greater than those of the  $A_{12}$ ,  $A_{13}$  modes. The phase velocities of the class A supersonic instability waves are given in figure 23. In this figure, the waves with maximum spatial growth rates are indicated by a small circle. Their values are nearly the same as their two-dimensional counterparts shown in figure 9.

The dispersion relations of the m=1 three-dimensional class C and D neutral

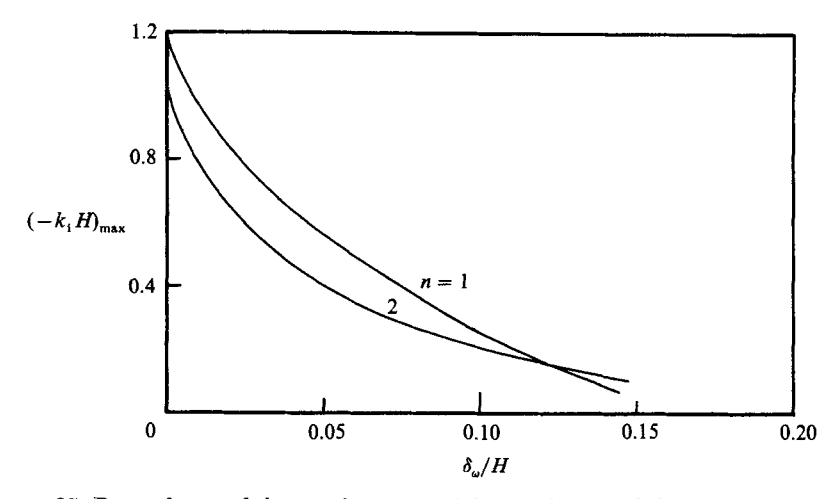


FIGURE 25. Dependence of the maximum spatial growth rate of the  $A_{11}$  and  $A_{12}$  mode instability waves on vorticity thickness of the shear layer.  $M_1=4.5({\rm He}),~M_2=1.6({\rm N_2}),~H_1=H_2=\frac{1}{2}B,~\bar{a}_1/\bar{a}_2=1.29.$ 

waves are similar to their two-dimensional counterparts. As beofre, class C waves are linked to class B instability waves. Both families are waves produced primarily by reflections off the top wall of the rectangular channel. On the other hand, class A and D waves are formed mainly by reflections off the bottom wall. Figure 24 shows typical eigenfunction (pressure) distributions of class A supersonic instability waves at the maximum growth rate over the entire height of the channel. In the lateral direction, the distribution has a cosine function dependence. Qualitatively, figures 24 and 13 are very similar. This similarity is also true, although not shown here, for class B, C and D waves.

The effect of finite shear-layer thickness on the growth rate of three-dimensional supersonic instability waves is shown in figure 25. In this figure the variations of the maximum growth rates of the  $A_{11}$ ,  $A_{12}$  modes are given as functions of the vorticity thickness of the shear layer. As can easily be seen the growth rates of these threedimensional waves decrease rapidly with increase in shear-layer thickness. The rate of decrease is faster than those of the corresponding two-dimensional wave modes (see figure 17). At  $\delta_{\omega}/H \geqslant 0.1$  the lowest-order two-dimensional mode, namely the  $A_{01}$  mode, has the highest spatial growth rate. The implication appears to be that the  $A_{01}$  mode probably constitutes the most dominant instability wave in a realistic situation. Based on this result it is, therefore, justified, as has been assumed in the present study, to confine one's primary attention to the low-order, low-dimension instability wave modes. The variation of the phase velocity of the most unstable wave of the  $A_{11}$  wave mode with the vorticity thickness of the shear layer has been calculated. Over the range of thickness calculated, the phase velocity is practically constant. As a matter of fact, it is numerically equal to that of the most unstable twodimensional ( $A_{01}$  mode) wave. This result strongly suggests that experimentally it would not be possible to distinguish between the two-dimensional and threedimensional instability waves by measuring the wave speeds alone.

## 5. Discussion

In this paper it is found that two-dimensional supersonic mixing layers inside a rectangular channel may undergo supersonic instabilities. These supersonic instability waves are generated by Mach wave systems formed by reflections from the channel walls. They exist only when the convective Mach numbers of the flow on both sides of the shear layer are supersonic. Two families of these supersonic instability waves have been identified. At supersonic convective Mach numbers these waves are the dominant instabilities of the flow. The growth rate of these instabilities, however, reduces as the thickness of the mixing layer increases. A complete normal mode analysis of such a flow has been carried out. The result reveals that the flow also supports two other families of neutral acoustic waves, one of which is generically related to the supersonic instability waves.

In the experiments of Papamoschou & Roshko (1986) and Chinzei et al. (1986) schlieren observations indicated clearly the existence of large-scale coherent structures (waves) in their confined supersonic shear layers. Here it is believed that these structures (waves) are the supersonic instability waves discussed in this paper. Unfortunately, other than the schlieren photographs, no other details and properties of these structures were measured. Thus a definitive confirmation of the present theoretical results is not possible at this time.

The concept that acoustic reflections could play a role in destabilizing a flow has been considered in the past by a number of authors in relation to the instabilities of cylindrical vortex-sheet jets. Gill (1965) appears to be the first to find and discuss these instabilities. However, instead of looking at the problem in the wave frame of reference and attributing the instability mechanism to the imbalance of in-phase pressure perturbations of the Mach wave systems as is done here, these authors proposed that the cause of instability was resonant reflections of acoustic waves at certain critical angles. Gill believed that at these critical angles of incidence the sound waves could trigger a large amount of energy release from the vortex sheet (mixing layer) which presumably would drive the instability. Recently Ferrari, Trussoni & Zaninetti (1981), Cohn (1983), Payne & Cohn (1984), Zaninetti (1986, 1987) and somewhat earlier Michalke (1970), following the suggestions of Gill, investigated the 'reflection modes' of these jets. Unfortunately, their studies were somewhat restricted and focused (except for Payne & Cohn) primarily on temporal instabilities. In addition, their calculated results also appear to be quite fragmentary. The present authors, Tam & Hu (1989), have since carried out spatial instability calculations of these jets using both vortex-sheet and more realistic finite-thickness mixing-layer models. Not surprisingly, certain instability wave modes were found to possess characteristics that were similar to the supersonic instability waves described in this paper.

This work was supported by the Office of Naval Research under Grant No. N00014-87-J-1130 and also in part by the Florida State University through time granted on its Cyber 205 Supercomputer.

## **Appendix**

Consider the vortex sheet in figure 3(a) as a rigid wall with vertical displacement  $y = \eta(x) = \epsilon \sin \alpha x$ . On starting from the linearized equations of motion it is easy to

show that the pressure disturbances  $p_1$  and  $p_2$  associated with the steady Mach wave systems above and below the wavy wall are governed by the equations

$$(M_{c1}^2 - 1)\frac{\partial^2 p_1}{\partial x^2} - \frac{\partial^2 p_1}{\partial y^2} = 0 \quad (y \geqslant 0), \tag{A 1}$$

$$(M_{c2}^2 - 1) \frac{\partial^2 p_2}{\partial x^2} - \frac{\partial^2 p_2}{\partial y^2} = 0 \quad (y \le 0),$$
 (A 2)

where  $M_{\rm c1}$  and  $M_{\rm c2}$  are the convective Mach numbers. The boundary conditions at the wavy wall are

 $\frac{\mathrm{d}\eta}{\mathrm{d}x} = \frac{v_1}{U_{c1}}, \quad \frac{\mathrm{d}\eta}{\mathrm{d}x} = -\frac{v_2}{U_{c2}}.$  (A3)

In (A 3)  $U_{\rm c1}$  and  $U_{\rm c2}$  are the mean flow velocities in the wave frame of reference and  $v_1$  and  $v_2$  are the y-components of the pertubation velocities. By means of the momentum equation, condition (A 3) may be rewritten in terms of the perturbation pressures as

$$\frac{\mathrm{d}^2 \eta}{\mathrm{d}x^2} = -\frac{1}{\rho_1} \frac{\partial p_1}{U_{c1}^2} \frac{\partial p_1}{\partial y}, \quad \frac{\mathrm{d}^2 \eta}{\mathrm{d}x^2} = \frac{1}{\rho_2} \frac{\partial p_2}{U_{c2}^2} \frac{\partial p_2}{\partial y}. \tag{A 4}$$

The boundary conditions at the top and bottom walls are

$$\frac{\partial p_1}{\partial y}(x, H_1) = 0, \quad \frac{\partial p_2}{\partial y}(x, -H_2) = 0. \tag{A 5}$$

It is straightforward to show that the solutions of the above boundary-value problems give a pressure difference,  $\Delta p = p_1(x, 0) - p_2(x, 0)$ , across the vortex sheet in the form

$$\frac{\Delta p}{\bar{p}} = \epsilon \alpha \left\{ \frac{\gamma_1 M_{\text{c1}}^2}{(M_{\text{c1}}^2 - 1)^{\frac{1}{2}}} \cot \left[ \alpha (M_{\text{c1}}^2 - 1)^{\frac{1}{2}} H_1 \right] + \frac{\gamma_2 M_{\text{c2}}^2}{(M_{\text{c2}}^2 - 1)^{\frac{1}{2}}} \cot \left[ \alpha (M_{\text{c2}}^2 - 1)^{\frac{1}{2}} H_2 \right] \right\} \sin \left( \alpha x \right), \tag{A 6}$$

where  $\bar{p}$  is the pressure of the mean flow. This is in phase with the displacement of the vortex sheet whenever  $\alpha$  is such that the coefficient of the expression on the right handside of (A 6) is positive.

#### REFERENCES

Blumen, W., Drazin, D. G. & Billings, O. F. 1975 Shear layer instability of an inviscid compressible fluid. Part 2. J. Fluid Mech. 71, 305-316.

Bogdanoff, D. W. 1983 Compressible effects in turbulent shear layers. AIAA J. 21, 926–927. Briggs, R. J. 1964 Electron-Stream Interaction with Plasmas. MIT Press.

CHINZEI, N., MASUYA, G., KOMURO, T., MURAKAMI, A. & KUDEN, K. 1986 Spreading of twostream supersonic turbulent mixing layers. *Phys. Fluids* 29, 1345-1347.

COHN, H. 1983 The stability of a magnetically confined radio jet. Astrophys. J. 269, 500-512.

FERRARI, A., TRUSSONI, E. & ZANINETTI, L. 1981 Magnetohydrodynamic Kelvin-Helmholtz instabilities in astrophysics II. Cylindrical boundary layers in vortex sheet approximation. Mon. Not. R. Astr. Soc. 196, 1051-1066.

GILL, A. E. 1965 Instabilities of Top-Hat jets and wakes in compressible fluids. Phys. Fluids 8, 1428–1430.

GROPENGIESSER, H. 1970 Study of the stability of boundary layers in compressible fluids. NASA TT-F-12, 786.

- IKAWA, H. & KUBOTA, T. 1975 Investigation of supersonic turbulent mixing with zero presure gradient. AIAA J. 13, 566-572.
- LANDAU, L. D. & LIFSHITZ, E. M. 1959 Fluid Mechanics. Addison-Wesley.
- LESSEN, M., Fox, J. A. & Zien, H. M. 1965 On the inviscid stability of the laminar mixing of two parallel streams of a compressible fluid. J. Fluid Mech. 23, 355-367.
- LIEPMANN, H. & PUCKETT, A. E. 1947 Introduction to Aerodynamics of a Compressible Fluid, pp. 239-241. Wiley.
- LIEPMANN, H. & ROSHKO, A. 1957 Elements of Gas Dynamics. Wiley.
- MICHALKE, A. 1970 A note on the spatial jet instability of the compressible cylindrical vortex sheet. DFVLR FB 70-51.
- MILES, J. W. 1958 On the disturbed motion of a plane vortex sheet. J. Fluid Mech. 4, 538-552.
- Papamoschou, D. & Roshko, A. 1986 Observations of supersonic free shear layers. AIAA Paper 86-0162.
- Payne, D. G. & Cohn, H. 1985 The stability of confined radio jets: the role of reflection modes. Astrophys. J. 291, 655-667.
- Tam, C. K. W. & Hu, F. Q. 1989 On the three families of instability waves of high speed jets. J. Fluid Mech. 201, 447-483.
- TAM, C. K. W. & MORRIS, P. J. 1980 The radiation of sound by the instability waves of a compressible plane turbulent shear layer. J. Fluid Mech. 98, 349-381.
- Zaninetti, L. 1986 Numerical results on instabilities of top hat jets. *Phys. Fluids* 29, 332-333.
- Zaninetti, L. 1987 Maximum instabilities of compressible jets. Phys. Fluids 30, 612-614.